Helix Mutations Stabilize a Late Productive Intermediate on the Folding Pathway of Ubiquitin[†]

Anita M. Rea, Emma R. Simpson,[‡] Maria D. Crespo,[§] and Mark S. Searle*

Centre for Biomolecular Sciences, School of Chemistry, University of Nottingham, University Park, Nottingham NG7 2RD, U.K.

Received April 23, 2008; Revised Manuscript Received June 5, 2008

ABSTRACT: We have investigated the relative placement of rate-limiting energy barriers and the role of productive or obstructive intermediates on the folding pathway of yeast wild-type ubiquitin (*wt*-Ub) containing the F45W mutation. To manipulate the folding barriers, we have designed a family of mutants in which stabilizing substitutions have been introduced incrementally on the solvent-exposed surface of the main α-helix (residues 23−34), which has a low intrinsic helical propensity in the native sequence. Although the U → I and I → N transitions are not clearly delineated in the kinetics of *wt*-Ub, we show that an intermediate becomes highly populated and more clearly resolved as the predicted stability of the helix increases. The observed acceleration in the rate of folding correlates with helix stability and is consistent with the I-state representing a productive rather than misfolded state. A Leffler analysis of the effects on kinetics of changes in stability within the family of helix mutants results in a biphasic correlation in both the refolding and unfolding rates that suggest a shift from a nucleation−condensation mechanism (weakly stabilized helix) toward a diffusion−collision model (highly stabilized helix). Through the introduction of helix-stabilizing mutations, we are able to engineer a well-resolved I-state on the folding pathway of ubiquitin which is likely to be structurally distinct from that which is only weakly populated on the folding pathway of wild-type ubiquitin.

An early observation in the field of protein folding was the notion that small proteins fold via two-state kinetics (*1*). Increasingly high resolution analyses have identified nonlinear rate profiles in both refolding and unfolding data which suggest deviations from this simple model that point to transiently populated intermediates or high-energy states indicative of much more rugged energy landscapes (*2–4*). Perturbation to kinetic barriers between species through alteration of refolding and unfolding conditions and through the introduction of point mutations, coupled with the development of instrumentation with faster time resolution, has shown that these species can be detected experimentally (*5–9*). However, it remains the case that a significant number of small proteins fold via an apparent two-state mechanism in which the native properties appear to rapidly accumulate in a concerted kinetic process of collapse and stabilization of secondary and tertiary interactions without significant population of an intermediate (*1*). This rate-limiting large-scale change in the topology of the polypeptide chain would appear to account for significant fractional changes in surface burial observed for many small proteins and the correlation between folding rate and various measures of folding topology (contact order) (*10*). Underpinning the apparent continuum of folding mechanisms is the relative placement of rate-limiting barriers along the various folding pathways, the relative energies of these barriers, and the stabilities of productive or obstructive intermediate states which determine whether such states become significantly populated.

Ubiquitin is a paradigm for folding studies (*11–16*), although attempts to unambiguously assign its folding pathway to either an apparent two-state model or a more complex multistate process have been complicated by the fact that the kinetics and mechanism of folding depend on the protein construct under investigation and the experimental conditions employed (*12*). The most recent studies (*17, 18*) have presented evidence of multiple refolding phases that are not eliminated in a proline-free mutant. We reported inconsistencies between equilibrium and kinetic stabilities and *m* values in studies of yeast ubiquitin, with further evidence from sequential mixing experiments suggesting both the population of an intermediate state and the possibility of kinetic partitioning which allows molecules to reach the native state along parallel (major and minor) folding pathways (*17*).

Vallée-Bélisle and Michnick (*18*) have described refolding studies using five different Trp probes positioned across the surface of ubiquitin to enhance the visibility of different folding transitions and probe both local and global changes

[†] A.M.R. and M.D.C. were supported by University Post-Graduate Research Scholarships and funding from the School of Chemistry, University of Nottingham, and E.R.S. was supported by a BBSRC Committee Studentship. M.D.C. acknowledges the financial contributions of Astex Technology Ltd. and Roche Products Ltd.

* To whom correspondence should be addressed. E-mail: mark.searle@nottingham.ac.uk. Telephone: (+44) 115 951 3567. Fax: (+44) 115 846 8002.

[‡] Current address: Lehrstuhl Biotechnologie, Department Chemie, Technische Universität München, Lichtenbergstrasse 4, 85747 Garching, Germany.

[§] Current address: Institute for Molecular Biology and Biophysics, ETH Zürich, Schafmattstrasse 20, 8093 Zürich, Switzerland.

10.1021/bi800722d CCC: $40.75
Published on Web 07/11/2008

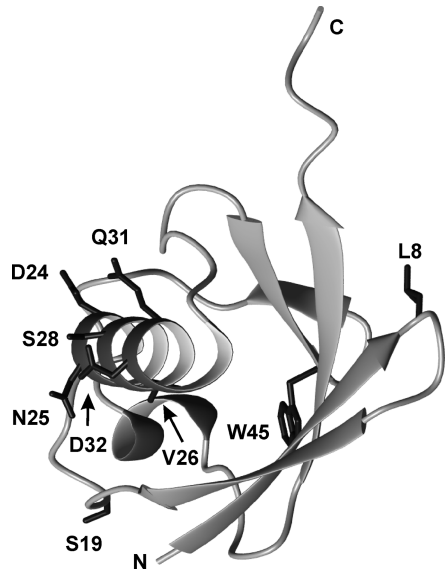

FIGURE 1: Ribbon structure of yeast ubiquitin showing the orientation of the main α-helix with the position of key residues illustrated. L8, D24, N25, S28, Q31, and D32 are largely solvent exposed; however, the side chain of V26 is buried in the hydrophobic core against the concave face of the β-sheet. The position of S19 (mutated to P in human ubiquitin) is shown in the loop connecting the second β-strand of the hairpin to the helix.

in the conformation of the polypeptide chain during folding. A number of these fluorescent reporters detected a significant population of an intermediate with the appearance of a pronounced rollover in the chevron plot. In other cases, there is also evidence for a burst phase in the fluorescence intensity at low concentrations of denaturant consistent with the accumulation of an early folded state within the dead time of the stopped-flow experiment. In the case of the widely used Trp45 fluorescent probe, the U → I and I → N transitions appear to be so poorly resolved that they merge to give an apparent U → N transition and a V-shaped chevron characteristic of a two-state mechanism (*11, 12, 17*). In contrast, Trp probes in other locations with different structural sensitivities are able to distinguish between the U → I and I → N transitions. A double mutant ($Ub^{F45W-T66W}$) displays fluorescence changes of opposite sign which are successful in resolving the two transitions within a single mutant (*18*). Ubiquitin mutants with enhanced fluorescence of the I-state were concluded to demonstrate that in these cases an intermediate is formed which is stable, compact, misfolded, and on the folding pathway.

We have investigated the nature of the folding intermediate of yeast *wt*-Ub in an alternative approach by incrementally stabilizing the protein by introducing substitutions into the main α-helix (Figure 1). In contrast to introducing large hydrophobic Trp residues into the structure, which have the potential for perturbing the folding dynamics of the native polypeptide chain by promoting hydrophobic collapse (*19*), we have introduced a number of mainly Ala mutations on the solvent-exposed surface of the helix. In this context, Trp45 proves to be a highly sensitive fluorescent probe for detecting the formation of multiple kinetic phases, consistent with an on-pathway intermediate state that becomes increasingly highly populated as the intrinsic stability of the helix increases. Moreover, the accelerated conversion of the I-state to the N-state in the mutants with the highest predicted helical propensity, coupled with estimates of the change in hydrophobic surface burial for each of the transitions, suggests that the I-state is compact and productive with regard to folding, rather than representing a misfolded state. We have analyzed the folding mechanism using a Leffler analysis of the family of helix mutants (*20*), which suggests a shift from a nucleation−condensation mechanism for *wt*-Ub, in which the native helix is weakly stabilized, toward a diffusion−collision model for the helix-stabilized mutants with a populated I-state. These mechanisms appear to represent different manifestations of the same unifying folding landscape of *wt*-Ub.

MATERIALS AND METHODS

Mutagenesis and Protein Expression. A pKK223-3 plasmid construct containing the F45W yeast ubiquitin gene was used as a template for mutagenesis reactions. Mutations were carried out using the QuikChange site-directed mutagenesis kit and confirmed by DNA sequencing. Proteins were expressed in *Escherichia coli* strain BL21(DE3) under the control of the IPTG-inducible *tac* promoter and purified as previously described (*21, 22*). Helical mutants were constructed, as illustrated in Figure 2.

NMR Analysis of the Helix Mutants. We analyzed a number of the helical mutants (*wt*-Ub, EA_3L, EA_4L, EA_4L-A28G, and EA_4L-A32G) in detail by NMR at 600 MHz on a Bruker Avance600 spectrometer equipped with a triple-resonance probe to verify that the sequence changes had not produced structural perturbations outside of the helical segment. Comparisons of Hα chemical shift deviations from random coil values ($\Delta\delta$Hα) show considerable similarities for each of the mutants both within the helical region and for flanking residues. The residues immediately N- and C-terminal to the helix, namely, T22, G35, and I36, suggest little structural perturbation. The significant differences between *wt*-Ub and the various mutants largely reflect the local effects of specific residue substitutions. The extent of helix formation is also defined well by patterns of NOEs at the N- and C-termini of the helix. Detailed comparison of the NOE data for *wt*-Ub and the mutants showed that these matched closely, suggesting that the increased helical stability has not distorted the helical boundaries.

Kinetic Experiments. Kinetic unfolding and refolding measurements were performed using an Applied Photophysics Pi-star 180 spectrophotometer, as described previously (*17, 21, 22*). The temperature was regulated using a Neslab RTE-300 circulating programmable water bath. All kinetic experiments were performed in 25 mM acetate buffer (pH 5.0) over the indicated range of temperatures. Refolding experiments were performed by 1:10 dilution of unfolded protein (15 μM in 5 M GdmCl) into buffered solutions of different GdmCl concentrations, yielding a final protein concentration of 1.36 μM. Experiments at a 5-fold lower dilution were performed to assess the possible contribution of protein aggregation on refolding rates, but no differences in rate constant were apparent. For unfolding experiments, a buffered solution of native protein was unfolded by a 1:10 dilution. Kinetic measurements for both unfolding and refolding reactions were averaged four to six times at each GdmCl concentration. In all cases, the GdmCl concentration was determined using a refractometer.

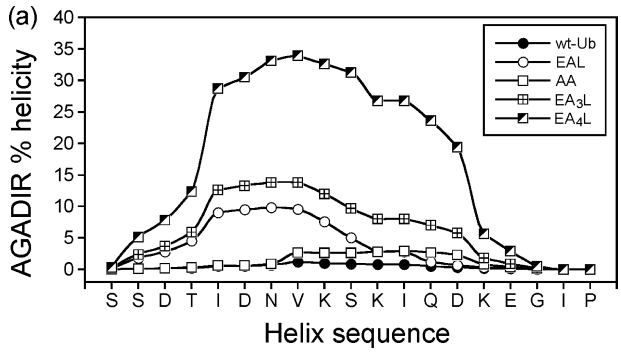

	Mutant	Helix sequence (20 25 30 35)
(b)	Wt-Ub	SSDTIDNVKSKIQDKEGIPP
	EAL	SSDTIEALKSKIQDKEGIPP
	AA	SSDTIDNVKSKIAAKEGIPP
	EA_3L	SSDTIEALKSKIAAKEGIPP
	EA_4L	SSDTIEALKAKIAAKEGIPP
	EA_4L-A28G	SSDTIEALKGKIAAKEGIPP
	EA_4L-A32G	SSDTIEALKAKIAGKEGIPP
(c)	Wt-Ub	SSDTIDNVKSKIQDKEGIPP
	N25G	SSDTIDGVKSKIQDKEGIPP
	S28G	SSDTIDNVKGKIQDKEGIPP
	D32G	SSDTIDNVKSKIQGKEGIPP
	N25G/D32G	SSDTIDGVKSKIQGKEGIPP
	GGG*	SSDTIDGVKGKIQGKEGIPP

FIGURE 2: (a) Analysis of the intrinsic helical propensity of the sequence of the main helix of *wt*-Ub (residues 19−38 included) using AGADIR. This is compared with a family of engineered helix mutants containing up to six specific stabilizing substitutions, as shown in panel b. The intrinsic helical propensity of the native sequence is very low (<2%); however, in the rationally stabilized mutants, this is predicted to increase to ∼35% in the case of EA_4L. (c) The sequences of three single-Gly helix mutants of *wt*-Ub, a double-Gly mutant, and a triple-Gly mutant (GGG*, representing N25G/S28G/D32G) are also shown, all of which are predicted to further destabilize the native helical sequence. Mutated residues are underlined.

Analysis of Kinetic Data. The kinetic data were analyzed using a multiexponential fitting procedure (typically three refolding phases and one unfolding phase were observed) with the quality of the fit determined from an analysis of the residuals. Chevron plots were constructed by plotting the natural log of the observed rate constants versus denaturant concentration (*23–25*). Chevrons for some of the *wt*-Ub data at 298 K in which a linear dependence of ln k_{obs} was observed were fitted using nonlinear regression analysis using Kaleidagraph according to the expression for a two-state (U ↔ N) transition:

$$\ln k_{obs} = \ln[k_{UN} \exp(-m_{UN}[D]/RT) + k_{NU} \exp(m_{NU}[D]/RT)] \quad (1)$$

Leffler plots (*20, 26*) were constructed to analyze the effects of point mutations on refolding and unfolding rates for some of the helical mutants of *wt*-Ub under apparent two-state conditions ($K_{UI} \ll 1$) assuming that

$$\ln k_{UN} = \ln k_{UN}^{\circ} - \alpha_f \Delta\Delta G_{UN}/RT \quad (2)$$

$$\ln k_{NU} = \ln k_{NU}^{\circ} + (1 - \alpha_f)\Delta\Delta G_{UN}/RT \quad (3)$$

where k_{UN}° and k_{NU}° are the rate constants for folding and unfolding for *wt*-Ub, respectively, k_{UN} and k_{NU} are the folding rates for the helix mutants derived from the chevron analysis, $\Delta\Delta G_{UN}$ is the change in stability, and α_f is a constant describing the degree of nativelike structure formation in the folding transition state.

Kinetic data which exhibited deviations from linearity in the denaturant dependence of the refolding rates (rollover effects) were fitted to both on-pathway (U ↔ I ↔ N) and off-pathway (I ↔ U ↔ N) three-state models (*25*). The observed rate constants and amplitudes were fitted simultaneously using the analytical solutions to the rate matrix describing the production and decay of the three species U, I, and N (*23*). The two observable macroscopic rate constants for the on-pathway mechanism (λ_1 and λ_2) are the positive and negative solutions to the quadratic

$$\lambda^2 + (k_{UI} + k_{IU} + k_{IN} + k_{NI})\lambda + (k_{UI}k_{IN} + k_{UI}k_{NI} + k_{IU}k_{NI}) = 0 \quad (4)$$

Data were analyzed globally using IGOR (Wavemetrics) by simultaneously fitting the normalized amplitudes of the refolding and unfolding processes to determine the microscopic rate constants. Amplitudes for the refolding phases of λ_1 and λ_2 were fitted to eqs 5 and 6 and the amplitudes for the unfolding phases of λ_1 and λ_2 to eqs 7 and 8, where F_I is the relative fluorescence intensity of the intermediate state (*23*).

$$A_1(\text{refolding}) = [F_I k_{UI}(\lambda_1 - k_{NI}) - k_{UI}k_{IN}]/[\lambda_1(\lambda_1 - \lambda_2)] \quad (5)$$

$$A_2(\text{refolding}) = [F_I k_{UI}(\lambda_2 - k_{NI}) - k_{UI}k_{IN}]/[\lambda_2(\lambda_1 - \lambda_2)] \quad (6)$$

$$A_1(\text{unfolding}) = [k_{NI}(\lambda_1 - k_{UI} - k_{IU}) + F_I k_{NI}(\lambda_1 - k_{UI})]/[\lambda_1(\lambda_1 - \lambda_2)] \quad (7)$$

$$A_2(\text{unfolding}) = -[k_{NI}(\lambda_2 - k_{UI} - k_{IU}) + F_I k_{NI}(\lambda_2 - k_{UI})]/[\lambda_2(\lambda_1 - \lambda_2)] \quad (8)$$

For the propagation of errors, those originating from the individual refolding and unfolding curves obtained at different denaturant concentrations were used. Errors quoted on subsequent calculations are those obtained directly from the IGOR global fitting procedure. A similar set of equations was derived for the off-pathway three-state mechanism (I ↔ U ↔ N). However, rate constants and amplitude data fitted to the on-pathway model gave more realistic values for the relative fluorescence intensity of the intermediate and lower errors.

The temperature dependence of the rate constants was analyzed to determine activation thermodynamic parameters ($\Delta H^{\circ\ddagger}$, $\Delta S^{\circ\ddagger}$, and $\Delta C_p^{\circ\ddagger}$) for the U → I and I → N transitions from the kinetic data for the helix-stabilized mutant EA_4L at denaturant concentrations between 0 and 2 M GdmCl and between 283 and 298 K (*27*). The rate constant k_{obs} is related to temperature by

$$\ln k_{obs} = \ln k_o - \Delta G^{\circ\ddagger}/RT \quad (9)$$

where k_o is the temperature-independent pre-exponential factor ($\sim 10^8$), with the temperature dependence of the activation free energy ($\Delta G^{\circ\ddagger}$) given by

$$\Delta G^{\circ\ddagger} = \Delta H^{\circ\ddagger} + \Delta C_p{}^{\circ\ddagger}(T - 298) - T[\Delta S^{\circ\ddagger} + \Delta C_p{}^{\circ\ddagger} \ln(T/298)] \quad (10)$$

Reported errors in these parameters reflect the quality of the nonlinear least-squares fit to the experimental data.

RESULTS

Engineering Stabilizing Substitutions in the Main Helix of wt-Ub. We have explored the folding pathway of yeast ubiquitin using the F45W background mutation as a fluorescent probe. We subsequently refer to this mutant as *wt*-Ub. The main helix (residues 23−34) packs within a concavity on the surface of the β-sheet forming a significant proportion of the hydrophobic core of *wt*-Ub (Figure 1) (*28*). A polypeptide corresponding to the isolated helix has been studied by NMR and CD in different solvents and, in agreement with helix−coil transition theory (*29*), appears to have a very low intrinsic helical propensity (<2%) (*30–32*). We used AGADIR to design a family of helix-stabilized mutants of yeast *wt*-Ub by introducing substitutions mainly on the solvent-exposed surface of the helix to alter secondary structure propensity without perturbing tertiary interactions or introducing non-native contacts that may result in the stabilization of misfolded states (Figure 2a).

The residues D24, N25, S28, Q31, and D32 have largely solvent-exposed side chains (Figure 1), allowing the helix stability to be increased via introduction of multiple mutations at these positions via substitution mainly with Ala. However, in the case of the D24E substitution, there was the possibility of introducing a helix-stabilizing salt bridge between the side chain of Glu24 and Lys27, which is present in the structure of the mammalian protein. We also introduced a substitution for the solvent inaccessible residue Val26 which is involved in core hydrophobic packing interactions between the α-helix and the β-sheet. Previous studies had suggested that the V26L mutation has a relatively small effect on stability (∼1 kJ/mol) with the Leu side chain readily accommodated through some small local adjustments to side chain packing (*14*). The AGADIR calculations suggest that the V26L substitution further enhances the helical propensity of this portion of the polypeptide chain. The complete family of helix mutants, containing between two and six substitutions, together with the nomenclature used, is shown in panels b and c of Figure 2. The AGADIR calculation of percentage helicity at each position is shown in Figure 2a for each of the stabilized mutants. From a background level of <2% in the native sequence, the most highly substituted mutant, EA_4L, has an estimated helicity of ∼35% (Figure 2a). Subsequently, we introduced Gly point mutations at various positions (A28G and A32G) to probe secondary structure formation in the transition state of the highly stabilized EA_4L mutant (see Figure 2) (*33, 34*).

Folding Kinetics for the Helix-Stabilized Mutants. The helical mutants were characterized by stopped-flow fluorescence at 283 K in 25 mM acetate buffer (pH 5.0). In all cases, the refolding data were resolved into three phases, only two of which (λ_1 and λ_2) show significant denaturant-dependent changes in rates and amplitudes. The variations with denaturant concentration are shown for AA, EAL, EA_3L, and EA_4L (Figure 3). The slowest phase, λ_3, represents <5% of the amplitude change and showed little variation in rate constants with refolding conditions (0.5−3 s^{-1}), suggesting a slow isomerization phase, as previously identified (*17, 21, 27*). To simplify the appearance of the data, neither λ_3 nor A_3 is included in the plots in Figure 3. In all cases, λ_1 has the highest amplitude ($A_1 > 0.8$) at low denaturant concentrations; however, there is a rapid crossover between A_1 and A_2 as the denaturant concentration increases, before A_2 finally decays to zero close to the midpoint of the chevron. This behavior is typical of a three-state model in which the I → N transition (λ_2) is associated with a significant rollover at low denaturant concentrations, consistent with formation of a stable I-state (*23*). Global fitting of all of the data (rate constants and amplitudes) is consistent with an on-pathway three-state model, with lines of best fit shown in Figure 3. The effects of the mutations on the stability of the intermediate (ΔG_{UI}) and on the native state (ΔG_{UN}) show that the mutants with the highest predicted helical propensities (EA_3L and EA_4L) have the most stable and highly populated intermediates (Table 1). The analysis demonstrates that under conditions in which the I-state is significantly populated the Trp45 mutation is a sensitive spectroscopic probe of both the U → I and I → N folding transitions.

We also globally fitted the experimental data to the three-state off-pathway model but obtained unrealistic values for the relative fluorescence intensity of the intermediate (F_I) as well as larger fitting errors. We further discriminated between on-pathway and off-pathway mechanisms using the approach described for cytochrome *c* on the basis of relative rate constants for λ_1 and λ_2 (*24, 35*). It has been shown that under conditions that favor the native state, the observed rate constant for the I → N transition can be slower than or equal to the microscopic rate constant for the I → U transition only in the on-pathway model. Consistent with this model, we observe that for EA_3L and EA_4L and the two EA_4L Gly mutants, where the data are well-resolved, $k_{IU} < k_{IN}$, supporting the on-pathway model.

Is the I-State Misfolded or a Productive Folding Species? The denaturant dependence of each of the rate constants provided *m* values from which we are able to estimate the relative extents to which hydrophobic surface area is buried in each of the transition states (TS1, U → I transition, and TS2, I → N transition) and the I-state. In all cases, k_{IU} and m_{IU}, which are associated with the I → U unfolding transition, are subject to the greatest uncertainty because of the low amplitude of these data. All other parameters are well-defined (see Table 1) with the rate constants for each transition showing clear differences between mutants that reflect their relative stabilities. In contrast, corresponding *m* values are quite similar, suggesting that the mechanisms are not changing significantly and that each of the key species (TS1, I-state, and TS2) is structured to similar extents for each of the mutants, with each species becoming progressively more compact. The I-state has β_I values between 0.67 and 0.77 and shows a variation in stability between the various stabilized mutants in the ΔG_{UI} range of −16.5 ± 0.5 to −23.3 ± 0.4 kJ/mol. This trend in I-state stability correlates with the trend in the estimated increase in helix propensity. The global fitting has enabled us to estimate a value for the fractional relative fluorescence intensity of the I-state (F_I), which lies in the range of 0.85−0.92 of that of the native state, indicating that the indole side chain of Trp45 is significantly solvent shielded in all of the mutants. Some

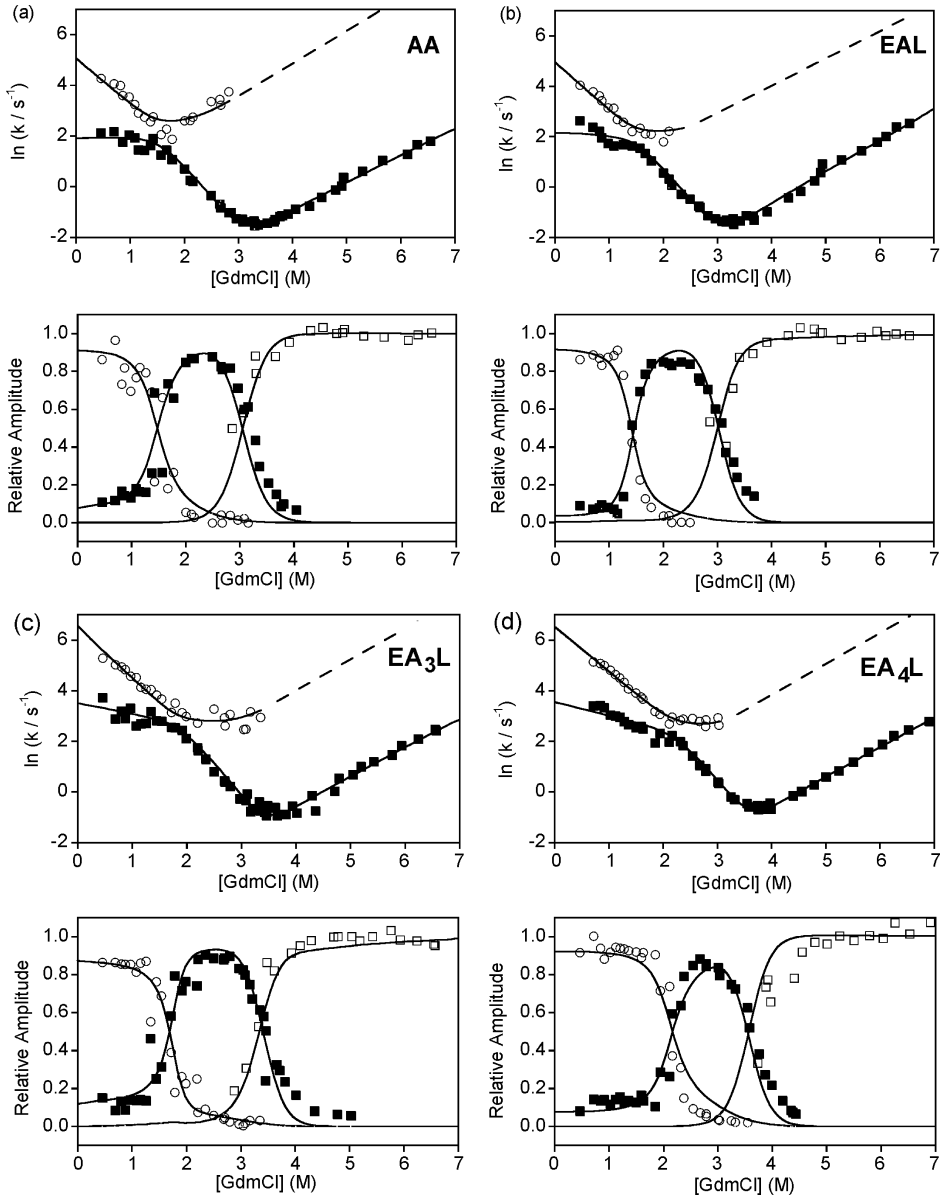

FIGURE 3: Denaturant dependence of the refolding and unfolding rate constants at 283 K for the helix-stabilized mutants AA (a), EAL (b), EA_3L (c), and EA_4L (d), with the corresponding amplitude variation of the two major phases for each mutant also shown. The amplitude of the fast phase (○) shows that the intermediate is significantly populated at low denaturant concentrations, resulting in a significant rollover for all mutants in the data for the I → N transition (■). The amplitudes of the two phases cross over at approximately 1.5−2 M GdmCl as the I-state is destabilized at increasing concentrations of denaturant. The lines of best fit for each mutant represent the global analysis of all of the data fitting to the three-state on-pathway model. In most cases, m_{IU} was poorly defined by either the low amplitude of the data or the lack of points and was fixed to 4.2 kJ mol^{-1} M^{-1} to optimize the global fit (Table 1).

difference between F_I and β_I may be expected since the former is a specific probe of the indole side chain environment whereas β_I provides a more global measure of hydrophobic surface burial.

The two folding transition states exhibit quite different properties. Values for β_{TS1} of ~0.4 suggest that the initial barrier to formation of a compact intermediate occurs early along the folding trajectory in terms of changes in solvent-excluded surface area. In contrast, the final barrier (TS2) defining the I → N transition is late, with β_{TS2} in the range of 0.76−0.80. The relative degree of surface exposure suggests that TS2 is associated with further compaction of the populated intermediate before reaching the native state. The recent studies with other Trp mutants of ubiquitin (including Ub^{M1W}, Ub^{S57W}, and Ub^{T66W}) (*18*) have suggested that the late folding I-state is more compact than the final transition state, indicating that some residues in the I-state have to be unfolded for the polypeptide to reach TS2. This is manifested in the kinetic data for the I → N transition by a rollover with an initially small positive slope (positive m_{IN} value) indicative of I-state unfolding before refolding (*18*). All of our helical mutants demonstrate a rollover with a small negative slope in the initial part of the curve for the I → N transition (see Figure 3 and Table 1), showing a sequential increase in the degree of compactness along the folding pathway from TS1 to the I-state to TS2.

We examined the effects of helix stabilization on the height of the rate-limiting barrier to folding. The kinetic data for the AA, EAL, EA_3L, and EA_4L mutants show that increasing the helical propensity leads to an increase in the stability of the I-state, but also to an acceleration of the rate of folding, suggesting that helix stability is having an even stronger

Table 1: Kinetic Parameters for the Refolding and Unfolding of *wt*-Ub and Various Helix-Stabilized Mutants at 283 K

variant	k_{UI} (m_{UI})	k_{IU} (m_{IU})[f]	k_{IN} (m_{IN})	k_{NI} (m_{NI})	ΔG_{UI}[c]	ΔG_{UN}[d]	F_I[b]	β_{TS1}[e]	β_I[e]	β_{TS2}[e]
wt-Ub[a]	–	–	103.0 ± 8.9 (−6.02 ± 0.1)	0.0022 ± 0.0002 (2.89 ± 0.06)	–	−25.3 ± 0.4	0.68	–	–	–
AA	159.6 ± 20.6 (−4.3 ± 0.2)	0.14 ± 0.01 (4.2)	6.9 ± 0.9 (−0.07 ± 0.2)	0.006 ± 0.001 (2.52 ± 0.09)	−16.5 ± 0.5	−33.1 ± 1.2	0.92	0.38	0.77	0.77
EAL[e]	145.0 ± 14.4 (−4.6 ± 0.2)	0.058 ± 0.009 (4.2)	9.12 ± 0.94 (−0.4 ± 0.2)	0.004 ± 0.001 (2.87 ± 0.07)	−18.4 ± 0.6	−36.6 ± 2.3	0.92	0.38	0.72	0.76
EA$_3$L	678.2 ± 82.6 (−4.8 ± 0.2)	0.043 ± 0.006 (4.2)	33.7 ± 4.1 (−1.0 ± 0.2)	0.006 ± 0.002 (2.69 ± 0.12)	−22.7 ± 0.6	−43.0 ± 1.9	0.88	0.38	0.71	0.79
EA$_4$L	668.0 ± 51.7 (−4.2 ± 0.1)	0.033 ± 0.003 (4.2)	34.4 ± 2.7 (−0.9 ± 0.02)	0.004 ± 0.001 (2.88 ± 0.07)	−23.3 ± 0.4	−44.6 ± 1.3	0.93	0.34	0.69	0.76
EA$_4$L-A28G	316.5 ± 43.0 (−4.3 ± 0.2)	0.064 ± 0.008 (4.2)	21.1 ± 2.9 (−1.2 ± 0.2)	0.003 ± 0.001 (2.86 ± 0.12)	−20.0 ± 0.6	−40.9 ± 1.8	0.89	0.35	0.67	0.77
EA$_4$L-A32G	371.4 ± 50.2 (−4.5 ± 0.2)	0.020 ± 0.002 (4.2)	24.1 ± 3.4 (−1.3 ± 0.2)	0.015 ± 0.004 (2.48 ± 0.12)	−23.2 ± 0.5	−40.5 ± 1.0	0.85	0.36	0.70	0.80
L8W	110.1 ± 9 (−5.5 ± 0.1)	0.059 ± 0.02 (4.2)	2.27 ± 0.3 (1.8 ± 0.3)	0.0012 ± 0.001 (2.21 ± 0.2)	−17.7 ± 0.9	−35.5 ± 2.8	0.90	0.54	0.96	0.78

[a] Values as fitted to a two-state system corresponding to k_{UN}, k_{NU}, and ΔG_{UN}. [b] A measure of the relative fluorescence of the intermediate where a value of 1 indicates the fluorescence of the intermediate is identical to that of the native state and a value of 0 indicates similarity to the denatured state. [c] $\Delta G_{UI} = -RT \ln(K_{UI})$. [d] $\Delta G_{UN} = -RT \ln[K_{UI}(k_{IN}/k_{NI})]$; both ΔG_{UI} and ΔG_{UN} are measured in kilojoules per mole. [e] β values were calculated as follows: $m_{kin} = m_{IU} - m_{UI} + m_{NI} - m_{IN}$; hence, $\beta_{TS1} = -m_{UI}/m_{kin}$, $\beta_I = (m_{IU} - m_{UI})/m_{kin}$, and $\beta_{TS2} = (m_{kin} - m_{NI})/m_{kin}$. [f] m values for the I → U transition were in many cases poorly defined by the data. This parameter was fixed at 4.2 kJ mol^{-1} M^{-1} in the fitting to optimize the global fit. β values were calculated accordingly.

FIGURE 4: Kinetic data for λ_2 for the helix-stabilized mutants plotted under approximate two-state conditions. Chevron plots represent a simple two-state analysis of the folding data and were constructed by fitting only the data that showed a linear dependence on denaturant concentration. The data points that result in rollover effects were not included in the analysis. In panel a, the data for *wt*-Ub and the four mutants, AA, EAL, EA$_3$L, and EA$_4$L, show the effects of increasing helix stability on the chevron. The most stable mutant, EA$_4$L, exhibits the fastest refolding rate. The strongest effects of the increase in stability are manifested in changes in the refolding and not the unfolding rates. (b) Similar analysis of the data for *wt*-Ub, EA$_4$L, and the two Gly mutants of EA$_4$L, namely, EA$_4$L-A28G and EA$_4$L-A32G, again showing the strongest effects of the mutations on the refolding rates.

effect in modulating the height of the rate-limiting barrier. For the purposes of illustration, we considered the kinetic data for the mutants under approximately two-state conditions at denaturant concentrations where the intermediate is destabilized. These data are fitted to a linear chevron plot in Figure 4a for illustration and clearly demonstrate that helix stabilization correlates with accelerated refolding rates. A similar approach was used to analyze the effects of the A28G and A32G mutations on A$_4$L (Figure 4b).

Thus, although the I-state is stabilized by substitutions within the helix, we also see a stabilization of TS2 which has the overall effect of accelerating folding. The observation that the stabilization of secondary structure has a beneficial effect on the folding kinetics appears to demonstrate that a productive intermediate is being formed rather than a misfolded state that must subsequently unfold to reach the final transition state. In contrast, the predicted consequence of the stabilization of a misfolded I-state, which has little effect on the stability of TS2, would be to increase the rate-limiting barrier to folding, resulting in a deceleration of the folding rate. The latter scenario has been proposed for the Trp mutants in the studies of Vallée-Bélisle and Michnick and is supported by the observation that the I-state is more compact than TS2 (*18*). The differences apparent in the two studies suggest that the hydrophobic nature of the Trp mutations themselves may have some perturbing influence in facilitating polypeptide chain collapse stabilized by non-native contacts.

Intermediate Formation in Native wt-Ub Monitored Using the F45W Mutation. The series of helix-stabilized mutants

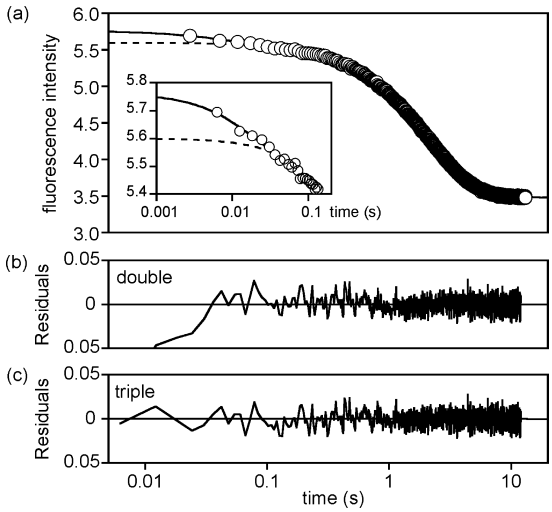

FIGURE 5: (a) Raw fluorescence decay data for *wt*-Ub at 283 K for refolding in 1 M GdmCl at pH 5.0. The fit to a double and triple exponential is shown along with the quality of the fit in each case, represented by the residuals shown in panels b and c. A fast phase is clearly evident in the double-exponential fit which is required to fully define the initial fluorescence decay. The triple-exponential fit fully describes the data, resulting in random residuals (c). The derived rate constants are 219 ± 46, 4.7 ± 0.02, and 0.75 ± 0.04 s^{-1}.

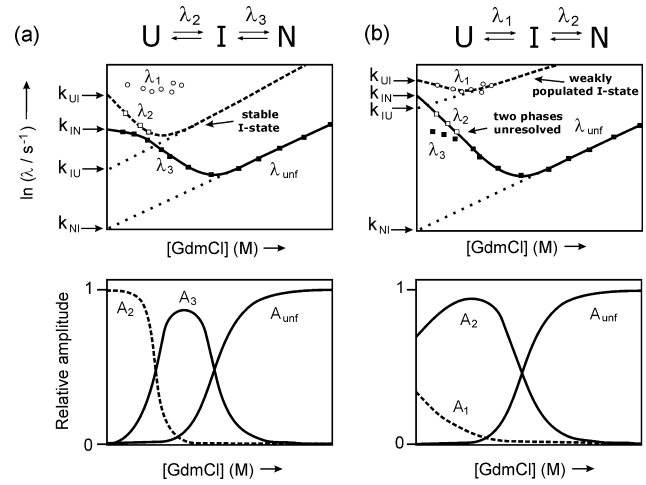

FIGURE 6: Schematic representation of the kinetic data for *wt*-Ub with the F45W mutation showing two possible scenarios for the analysis of the data. In the first case (a), the intermediate is significantly populated resulting in a well-defined increase and decay of the amplitude curve corresponding to the I → N transition (λ_3). The barriers for the U → I and I → N transitions merge such that the two rate constants are difficult to resolve at high denaturant concentrations. In the second case (b), the I-state is relatively weakly populated and a number of ill-defined data points with fast rates (λ_1) account for its rapid formation (U → I) and decay. The amplitude profile is quite different, with that of the fast phase (λ_1), corresponding to the rapid U → I transition, being very small and decreasing further as the denaturant concentration increases.

described above have enabled us to characterize a populated intermediate using the background F45W mutation as the fluorescent probe. Both the U → I and I → N transitions are resolved even though the TS1 and TS2 barrier heights appear to converge ultimately to yield rate constants for the U → I and I → N transitions that are indistinguishable. We re-examined the data for *wt*-Ub with the F45W mutation to determine whether there is clear evidence for a highly populated late I-state (*17*).

We collected data for *wt*-Ub under conditions identical to those described for the helix mutants (at 283 K), where the slower folding rates facilitated better resolution of the two folding transitions (see Figure 3). In the refolding data for *wt*-Ub at low denaturant concentrations (<2 M GdmCl), we were able to resolve either two or three phases with rate constants between ca. 300 and 1 s^{-1}, as illustrated in Figure 5. The analysis requires a fast kinetic phase that accurately describes the first few points of the fluorescence decay, which is evident from the residuals calculated for double-exponential (b) and triple-exponential fits (c). These points are resolved well beyond the ~2 ms dead time of the instrument (see the inset of Figure 5a). The low amplitude of this phase means that the derived rate constants are subject to a greater degree of uncertainty and show a much less clear correlation with denaturant concentration. We have also identified this fast phase in studies of a destabilized T12A/T14A double mutant of *wt*-Ub; however, the fast phase is not evident in the kinetic data of other stabilized mutants of *wt*-Ub, including S19P (one of three mutations found in the mammalian variant of ubiquitin), or in the kinetic data collected on *wt*-Ub at 298 K (*17*), although here a burst phase in the fluorescence intensity is apparent. The two remaining phases (λ_2 and λ_3) in the 283 K data account for the majority of the amplitude change, with λ_2 being the predominant phase at low denaturant concentrations ($A_2 > 0.8$). However, the rate constants for λ_2 and λ_3 rapidly converge and are not resolved at denaturant concentrations above 1 M GdmCl. The kinetic analysis of λ_3 is further complicated by mixing with other low-amplitude phases associated with prolyl or nonprolyl *cis*−*trans* isomerization events which have similar rate constants (1−3 s^{-1}). Identical slow processes similar in amplitude are also evident in the data for all of the helix mutants, consistent with an underlying population of isomerization-limited folding pathways (*21, 27*).

In contrast to the data for the helix-stabilized mutants, where the fastest phase is well resolved and readily assigned to the U → I transition, the fastest phase in the refolding data for *wt*-Ub was associated with higher rate constants (≥150 s^{-1}) and a much smaller amplitude ($A_1 < 0.2$). We have analyzed the data using the two possible scenarios presented schematically in Figure 6. In the first instance (a), we have assumed that the fast phase (λ_1) for *wt*-Ub is associated with the formation of a low-stability I-state which is only transiently populated. When the sum of the amplitudes for all of the observed phases for *wt*-Ub at 283 K, including the data for the low-amplitude fast phase, are plotted against the fluorescence of the unfolded state, we see a linear extrapolation that suggests these three phases fully account for the fluorescence amplitude (data not shown). The possibility of an additional low-amplitude I-state on the folding pathway adds a further level of complexity to the analysis, and for this reason, we have focused only on the main folding phases, λ_2 and λ_3, which we ascribe to the U → I and I → N transitions. The convergence of λ_2 and λ_3 at approximately 1.5 M GdmCl, as shown in the experimental data in Figure 7, makes it difficult to clearly resolve these phases; however, the implication of this model is that the intermediate must be significantly populated, resulting in a pronounced rollover in the chevron plot (illustrated schematically in Figure 6a). The amplitude profiles for λ_2 (U → I) and λ_3 (I → N) are expected to be similar to those observed for the AA and EAL helix-stabilized mutants shown in Figure

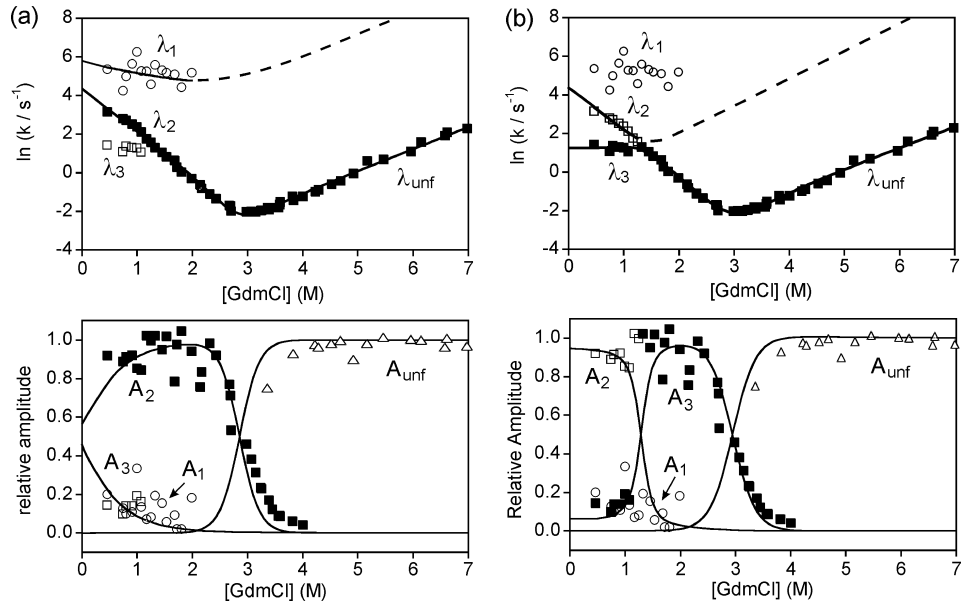

FIGURE 7: Kinetic analysis of the folding of *wt*-Ub at 283 K. (a) The kinetic data are resolved into three phases, λ_1, λ_2, and λ_3. The change in amplitude of these various phases as a function of denaturant concentration is also shown. The fastest phase λ_1 (which is not visible in the data at 298 K) is of low amplitude ($A_1 < 0.2$) and results in considerable scatter in the denaturant dependence of the rate constants. The lines of best fit have been determined from a global analysis of the data fitted to an on-pathway three-state model with a weakly populated I-state (see Figure 6b). For clarity, the amplitude data for λ_3 (which is low and independent of denaturant concentration) are not shown. In panel b, the same data set is fitted to the model shown in Figure 6a, in which the I-state is significantly populated. The data points for λ_3 are now accommodated by the main refolding phase and represent the rollover in the data for the I → N transition. The expected crossover in the amplitudes of A_2 and A_3 is less readily apparent.

3. As the two phases merge at approximately 1.5 M GdmCl, we anticipated a crossover in A_2 and A_3 as the I → N transition begins to dominate the change in fluorescence intensity (represented in Figure 6a). The experimental data shown in Figure 7a do not clearly show the crossover of the relative amplitudes of A_2 and A_3 predicted by this model which is evident in the data of the helix mutants (Figure 3). In Figure 7a, we have fitted both the rate and amplitude data to this model, based upon a significantly populated I-state. Although the rate constants produce a satisfactory fit, the crossover in the amplitudes is less convincing.

In the alternative scenario (Figure 6b), we fitted the data to a model in which the I-state is only weakly populated, with the U → I transition defined by the low-amplitude fast phase, λ_1. The scatter in the data for this phase precludes a detailed quantitative fit; however, the experimental amplitude changes are consistent with this model (Figure 7b). The main folding phase (λ_2; I → N transition) dominates the kinetics, showing a decrease in amplitude toward the midpoint of the transition (~3 M GdmCl) as contributions from the unfolding kinetics become more significant. The initial small increase in the amplitude for the I → N transition (A_2) at low denaturant concentrations reflects the destabilization of the weakly populated I-state, resulting in a very small (barely visible) rollover in the main chevron plot. Consistent with this, the amplitude of λ_1 (U → I transition) is very low ($A_1 < 0.2$) and continues to decrease as the I-state is destabilized. However, all of the low-amplitude phases exhibit some scatter. The remaining data for λ_3, representing the isomerization phases and other possible minor parallel folding pathways (*17*), similarly have a low amplitude and show very little variation with denaturant concentration. Thus, the data fit globally to both models, and there is some remaining ambiguity in distinguishing between them.

The Position of the Fluorescent Probe Affects I-State Stability. In parallel studies with those recently described by Vallée-Bélisle and Michnick (*18*), we considered how the visibility of the I-state was influenced by the location of the fluorescent probe by relocating the Trp mutation to the turn sequence in the N-terminal β-hairpin. The L8W mutation in *wt*-Ub produces a large increase in fluorescence intensity for the folding transition, in contrast to the decrease observed for Trp45. We analyzed the folding kinetics of L8W at 283 K under conditions otherwise identical to those described in the legends of Figures 3 and 7 for the helix mutants and *wt*-Ub with the Trp45 probe. The refolding data for L8W resolved into two phases at denaturant concentrations of <1.5 M GdmCl, with the two rate constants indistinguishable at higher concentrations. The unfolding data are described well by a single-exponential fit. Global fitting of the kinetic data and the amplitude changes for the two observed refolding phases shows that the folding mechanism of L8W is consistent with a three-state on pathway model with the crossover in A_1 and A_2, representing the U → I and I → N transitions (Figure 8,) characteristic of the behavior observed for the helix mutants (Figure 3). Thus, the amplitude change for λ_2 (I → N transition) shows the same increase and crossover with λ_1 as the population of the I-state increases under conditions that strongly favor folding. The overall effect of shifting the fluorescent probe from F45W to L8W is to stabilize the U → N transition by ~10 kJ/mol. The I-state for L8W becomes highly populated with a stability ΔG_{UI} of ~17 kJ/mol. In contrast to the data for the helix mutants, we observe an initially positive slope for L8W for the denaturant dependence of k_{IN}, indicating that the intermediate must first unfold to reach TS2, suggesting that the I-state may be more compact than is evident for the helix mutants (Table 1). The data for L8W show the characteristics

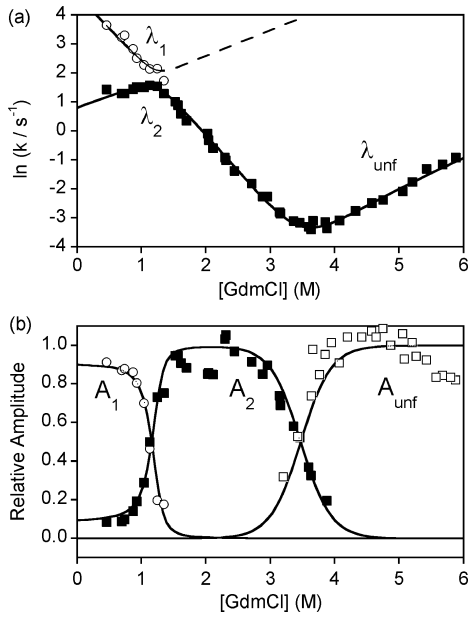

FIGURE 8: Kinetic data (amplitudes and rate constant dependence on denaturant concentration) for the L8W mutant at 283 K and pH 5.0 in acetate buffer. Two refolding phases are resolved which merge together at ~1.2 M GdmCl. The data are globally fitted to the three-state on-pathway model which confirms that a stable I-state is highly populated. A positive slope in the denaturant dependence of k_{IN} shows that the populated I-state is highly compact and must partially unfold in the U → TS2 transition. The data suggest that the I-state may represent a partially misfolded state stabilized by non-native interactions. The crossover of A_1 and A_2 is consistent with a highly populated I-state.

recently identified for a number of the Trp mutants described by Vallée-Bélisle and Michnick, and we concur that a highly populated and compact I-state is formed on the folding pathway which appears to represent a partially misfolded state (*18*). In contrast to the data presented above for the Trp45 mutant, where in one scenario we suggest that an I-state is only weakly populated, we are led to conclude that the visibility of the I-state of ubiquitin and at least some of its properties, including its stability and degree of compactness, are dependent on the influence of the Trp probe in stabilizing non-native hydrophobic contacts at different locations. The formation of an I-state stabilized by non-native contacts is less readily apparent in the helix-stabilized mutants where relatively small perturbations are introduced which appear to stabilize not only a compact I-state but also one which is productive for folding.

Thermodynamic Characterization of the Folding Transition States. The refolding phases for the U → I and I → N transitions at low denaturant concentrations are particularly well resolved for EA_4L and were studied as a function of temperature to provide thermodynamic insights into the structure of the two folding transition states, TS1 (U → I) and TS2 (I → N) (*21, 27*). Rate constants were determined at denaturant concentrations between 0 and 2 M GdmCl and exhibited a linear dependence at each of the temperatures studied between 283 and 298 K. The temperature dependence of ln k_{UI} and ln k_{IN} is shown in Figure 9. The curvature in the plot of ln k_{UI} shows that the rate constant varies very little over this temperature range, but significant changes are apparent for k_{IN}, indicating quite different thermodynamic profiles for the two transition states. The temperature dependence of the activation free energy for folding was

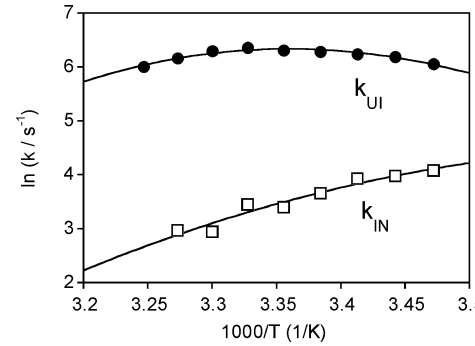

FIGURE 9: Temperature dependence of the rate constants k_{UI} and k_{IN} for the helix-stabilized mutant EA_4L collected over the temperature range of 283−298 K. The curved plots were fitted to eqs 9 and 10 to determine the activation parameters for folding.

determined using a pre-exponential factor k_o of 10^8 and enabled us to calculate the change in enthalpy ($\Delta H^{o\ddagger}$), entropy ($\Delta S^{o\ddagger}$), and heat capacity ($\Delta C_p^{o\ddagger}$) for transition state formation (*27*). While $\Delta H^{o\ddagger}$ and $\Delta C_p^{o\ddagger}$ are relatively insensitive to the estimated value of k_o, $\Delta S^{o\ddagger}$ can change significantly. In this context, we are concerned less with absolute values than with relative values for the activation parameters for the two transition states. The U → I transition is associated with a large negative change in heat capacity (-4.4 ± 0.5 kJ mol^{-1} K^{-1}) and a positive entropy change ($+121 \pm 26$ J K^{-1} mol^{-1}), both of which are typically associated with solvent expulsion, but overall a small enthalpy change (-1.3 ± 1.4 kJ/mol). The thermodynamic parameters suggest an initial barrier crossing event in which formation of the compact I-state is associated with hydrophobic collapse. In contrast, the I → N transition has a much smaller change in heat capacity (-1.9 ± 2.2 kJ mol^{-1} K^{-1}) but is strongly enthalpy-driven (-53.9 ± 6.2 kJ/mol) and opposed by a large adverse change in entropy (-204 ± 104 J K^{-1} mol^{-1}). This thermodynamic signature is consistent with the consolidation and further stabilization of the already compact intermediate state as the final rate-limiting barrier is crossed en route to the native state. The large enthalpy change appears to reflect van der Waals packing of side chains in the hydrophic core which is simultaneously associated with the loss of backbone and side chain dynamics as native side chain interactions are stabilized.

Degree of Helix Formation in the Transition State for Folding of the Stabilized Mutants. We have used the classical rate-equilibrium free energy relationship (REFER) to analyze the effects of incremental changes in equilibrium stability on the folding kinetics and structure of the rate-limiting transition state (*20, 36*). The slope α_f of this multipoint Leffler plot, which correlates ln(k_{UN}) and ln(k_{NU}) with $\Delta\Delta G_{UN}/RT$, provides a description of noncovalent bond formation in the transition state and has been applied in this context to establish the degree of structure formation both within the native helical sequence and in the engineered mutants which are predicted to have a much higher intrinsic helical propensity. A linear Leffler correlation provides an indication that the stability of the element of structure changes in a concerted manner during the folding reaction without significantly altering the structure of the transition state. Changes in slope α_f have also been identified that are consistent with shifts between competing parallel folding

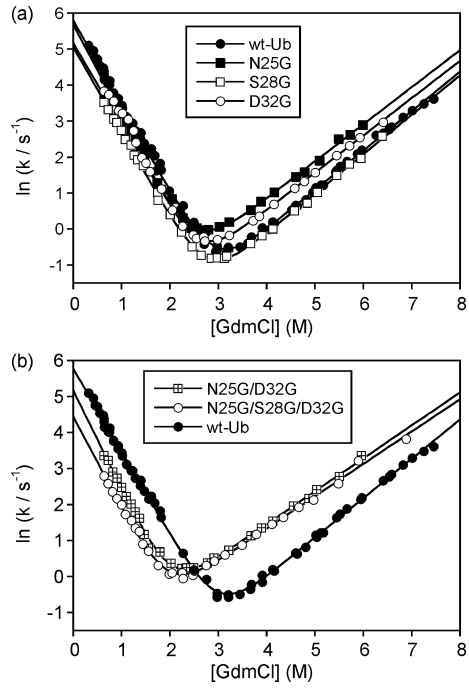

FIGURE 10: Kinetic data for the helix-destabilized mutants of *wt*-Ub. The data for the three single-point mutations are shown in panel a and give linear chevron plots indicative of approximately two-state folding kinetics. The data show qualitatively that changes in stability result in slightly greater effects on the unfolding rates. In panel b, the kinetic data for the double and triple helix mutants with Gly substitutions are compared with those for *wt*-Ub. Changes are apparent in both refolding and unfolding rates with a small change in the slope of the unfolding data suggesting that the transition state for folding for these highly destabilized mutants is shifting toward a more nativelike structure with an increase in β_{TS}.

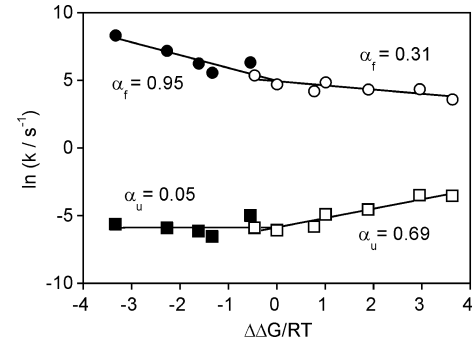

FIGURE 11: Leffler plot of the rates of refolding and unfolding of the helical mutants vs stability. The data for the family of helix-stabilized mutants are shown as black symbols. Both the refolding and unfolding data are biphasic. The refolding data for the helix-stabilized mutants are described by a slope α_f of 0.95 ± 0.21, which demonstrates that on average the helix is highly structured in the folding transition state of these mutants. In contrast, the refolding data for the destabilized mutants (○; from data in Figure 10) give a much shallower slope (α_f = 0.31 ± 0.06), suggesting that the helix is significantly less well structured and more diffuse, in agreement with the low intrinsic helical propensity of the native helix.

pathways (*20*) and Hammond-like movements (*37–39*) of the position of the transition state across a broad energy plateau.

The kinetic data were analyzed at denaturant concentrations where the I-state was not significantly populated (*20*), approximating to a simple two-state folding reaction ($k_{obs} = k_{UN} + k_{NU}$) with the data fitted to a linear chevron plot (Figure 4a). It is apparent that helix stabilization has the strongest effect in accelerating the refolding rate k_{UN}. The introduction of the A28G and A32G mutations into EA_4L similarly produced significant changes in the refolding rates (Figure 4b). We also generated a family of mutants of *wt*-Ub with destabilizing Xaa → Gly substitutions (N25G, S28G, S28A, and D32G) set against the background sequence of the native helix (Figure 2c). We further extended the stability range by introducing the double (N25G/D32G) and triple (N25G/S28G/D32G) Gly mutations (GGG* in Figure 2c). The linear chevron plots for the major folding phases for each mutant are shown in Figure 10. In this case, a qualitative analysis shows that in the majority of cases any changes in stability produced by the mutations appear to most significantly affect the unfolding rates. The single-point mutations (Figure 10a) have little effect on the *m* values in either the refolding or unfolding arms of the chevron plots and give calculated β_{TS} values (0.68−0.70) similar to those for the helix-stabilized mutants shown in Figure 4. However, the more destabilizing double and triple mutants led to a smaller slope corresponding to m_{NU} (Figure 10b), indicating that the transition state is becoming more nativelike and occurring later along the reaction coordinate (β_{TS} values of 0.73−0.75).

We constructed a Leffler plot for all of the mutants, representing a range of stabilities of ~16 kJ/mol and a >10-fold variation in refolding rates. The Leffler plots of $\ln(k_{UN})$ and $\ln(k_{NU})$ versus $\Delta\Delta G_{UN}/RT$ both show a significant deviation from a single linear correlation (Figure 11). Moreover, the data do not appear to be well-defined by a smooth curvature but by a biphasic behavior that divides the data into two groups corresponding to the effects of stabilizing and destabilizing mutations (*20*). The change in stability of the destabilized *wt*-Ub mutants fits well to a linear correlation with an α_f of 0.31 ± 0.06. The multipoint analysis suggests that on average the helix is only weakly stabilized in the transition state, consistent with the predicted low intrinsic helical propensity of <2% for *wt*-Ub (see Figure 2). However, when we analyzed the data for the helix-stabilized mutants (including the A28G and A32G mutants of EA_4L), we see a much larger slope in the refolding data with an α_f of 0.95 ± 0.21, indicating that on average the helix is now significantly more structured in the folding transition state.

DISCUSSION

Populated Intermediates in the Folding of Ubiquitin: Misfolded or Productive? Whether an I-state is populated on the folding pathway of ubiquitin has for some while been an issue of contention (*11–18*). Early evidence for a burst phase in the fluorescence intensity data came from a number of studies (*14*), indicative of a rapid transition in the dead time of the stopped-flow experiments characteristic of a weakly populated intermediate. Transient protein aggregation was subsequently shown to influence the folding kinetics (*12*). Further, the burst phase first proposed by Roder et al. (*14*) was not identified in a subsequent study by Krantz and Sosnick (*11*). Some of the recently described Trp mutants appear to show evidence of burst phase behavior (M1W, A28W, and T66W) (*18*), although this was not apparent in the analysis of the F45W mutant. Thus, there has not been

any consistency in the reported appearance of a burst phase in the F45W *wt*-Ub data, highlighting the difficulties in assigning burst phase amplitudes when considering rate processes approaching the instrumental dead time (*40*). Continuous-flow experiments described by Roder et al. (*48*) have further suggested fast processes (150 μs to 2 ms) occurring well within the dead time of conventional stopped-flow instrumentation (*40*). In contrast, the small-angle X-ray scattering (SAXS) measurements of Sosnick and Krantz (*15*), together with their earlier kinetic studies with mammalian ubiquitin (*11*), argued against a significant accumulation of secondary structure in the first few milliseconds of folding. Moreover, the observation of burst phase CD signals that might be construed as evidence of chain collapse within the dead time of the experiment were attributed to the response of the unfolded state to changes in solvent conditions that affect the distribution of backbone torsion angles. Hydrogen exchange experiments also suggested that there is no significant stabilization of secondary structure during the dead time of the stopped-flow experiment in advance of the main cooperative folding transition (*44*). Other studies have suggested the early formation of a compact structured ensemble without a fluorescence signature (*42*), and that multiple probes reveal the formation of nativelike intermediates during low-temperature refolding studies (*43*).

In recent studies, tryptophan probes were engineered at five different positions in ubiquitin to enhance the visibility of different folding transitions involving both local and global changes in the conformation of the polypeptide chain (*18*). A significant population of an I-state associated with a pronounced rollover in the chevron plot was detected for a number of these Trp mutants (M1W, S57W, and T66W); however, others appeared to be relatively "silent", including the widely used F45W mutation and A28W. The data for the F45W mutant appear to be ambiguous with the U $\rightarrow$ I and I $\rightarrow$ N transitions suggested to be so poorly resolved that values for k_{UI} and k_{IN} merge to give an apparent U $\rightarrow$ N transition and a V-shaped chevron that has been widely characterized up to this point as evidence of a two-state mechanism (*11, 12, 17*). However, on the basis of the global analysis presented here for Trp45 *wt*-Ub, and previous studies (*17*), the case for the population of a highly stabilized I-state is not clear-cut. However, the mutants M1W and S57W more clearly resolved a highly collapsed state driven by non-native interactions that must partially unfold in the final rate-limiting transition state (*18*). In contrast, our helical mutants demonstrate a rollover with a small negative slope in the initial part of the chevron for the I $\rightarrow$ N transition (see Figure 3 and Table 1), demonstrating that the I-state is less compact than the rate-limiting transition state. We have rationalized the data in terms of a sequential increase in hydrophobic surface burial along the folding pathway from U to TS1 to I to TS2 to N. The differences highlighted by the two studies suggest that the misfolded I-state reported to be stabilized by the Trp substitutions (ref *18* and this work), which leads to the requirement for error repair in the rate-limiting transition state, is structurally distinct from the I-state populated by the helix mutants, which appears to be stabilized by nativelike interactions. Both of these approaches have engineered I-states that appear to be much more stable and compact than the weakly populated intermediate on the folding pathway of native *wt*-Ub, from which we also conclude that they are structurally distinct.

We have shown in this investigation that by engineering stabilizing mutations on the solvent-exposed surface of the main helix an I-state becomes highly populated. The interactions that are stabilizing the I-state also appear to stabilize the late transition state, leading to an acceleration of the conversion of I to N. On this basis, we conclude that nativelike contacts are enhanced in the transition state by the stabilized helical template, rather than by non-native interactions which of necessity would have to be corrected by partial unfolding. In the general context, hierarchical mechanisms in which stable elements of secondary structure are accreted may invariably lead to the population of an intermediate state. It has been proposed that within a unifying mechanism for protein folding, the propensity of the polypeptide chain to form elements of stable secondary structure is an important controlling influence in determining which of the classical folding pathways will be followed (*44–46*), the two extreme manifestations of which are the nucleation−condensation and diffusion−collision mechanisms. The biphasic nature of the Leffler analysis of the ubiquitin mutants presented in this study is consistent with a shift toward the latter as the autonomous stability of the isolated helical sequence increases (*26, 45*). In a number of studies, the accumulation of an I-state has been rationalized on the basis of the formation of non-native contacts with the stabilized helix (*46, 47*), requiring error repair in the rate-limiting transition state before nativelike structure can be established and consolidated. These cases have demonstrated that non-native interactions play a significant role in the folding of native states, and that a late barrier to folding may more generally represent rate-limiting error repair processes that are an inescapable consequence of the rugged energy landscape for folding (*46–50*). The proposed folding mechanism for helix-bundle immunity protein Im7 is one such case (*46*). A diffusion−collision process, as suggested for a number of helical proteins, results in a substantial number of non-native hydrophobic interactions that are proposed to stabilize helix−helix contacts in a populated intermediate, driven by the burial of the maximum number of hydrophobic side chains. Misfolding appears to arise as a consequence of a hierarchical folding process in which stable helices form rapidly and present a hydrophobic template against which non-native contacts can form. Although the helix-stabilized mutants of *wt*-Ub reported in this study also result in a highly populated I-state, an increase in local secondary structure propensity appears to assist folding by lowering the energy barrier for the rate-limiting step which we conclude must be by facilitating formation of nativelike contacts in the transition state.

REFERENCES

1. Jackson, S. E. (1998) How do small single-domain proteins fold? *Folding Des. 3*, R81−R91.
2. Whittaker, S. B. M., Spence, G. R., Grossmann, J. G., Radford, S. E., and Moore, G. R. (2007) NMR analysis of the conformational properties of the trapped on-pathway folding intermediate of the bacterial immunity protein Im7. *J. Mol. Biol. 366*, 1001–1015.
3. Sanchez, I. E., and Kiefhaber, T. (2003) Evidence for sequential barriers and obligatory intermediates in apparent two-state protein folding. *J. Mol. Biol. 325*, 367–376.
4. Latypov, R. F., Cheng, H., Roder, N. A., Zhang, J., and Roder, H. (2006) Structural characterization of an equilibrium unfolding intermediate in cytochrome c. *J. Mol. Biol. 357*, 1009–1025.
5. Gorski, S. A., Capaldi, A. P., Kleanthous, C., and Radford, S. E. (2001) Acidic conditions stabilise intermediates populated during the folding of Im7 and Im9. *J. Mol. Biol. 312*, 849–863.
6. Chiti, F., Taddei, N., Webster, P., Hamada, D., Fiaschi, T., Ramponi, G., and Dobson, C. M. (1999) Acceleration of the folding

of acylphosphatase by stabilization of local secondary structure. *Nat. Struct. Biol. 6*, 380–387.
7. Maki, K., Cheng, H., Dolgikh, D. A., and Roder, H. (2007) Kinetics of Staphylococcal Nuclease Studied by Tryptophan Engineering and Rapid Mixing Methods. *J. Mol. Biol. 368*, 244–255.
8. Mayor, U., Guydosh, N. R., Johnson, C. M., Grossmann, J. G., Sato, S., Jas, G. S., Freund, S. M. V., Alonso, D. O. V., Daggett, V., and Fersht, A. R. (2003) The complete folding pathway of a protein from nanoseconds to microseconds. *Nature 421*, 863–867.
9. Callender, R., and Dyer, R. B. (2002) Probing protein dynamics using temperature jump relaxation spectroscopy. *Curr. Opin. Struct. Biol. 12*, 628–633.
10. Plaxco, K. W., Simons, K. T., and Baker, D. (1998) Contact order, transition state placement and refolding rates of single domain proteins. *J. Mol. Biol. 277*, 985–994.
11. Krantz, B. A., and Sosnick, T. R. (2000) Distinguishing between two-state and three-state models for ubiquitin folding. *Biochemistry 39*, 11696–11701.
12. Went, H. M., Benitez-Cardoza, C. G., and Jackson, S. E. (2004) Is an intermediate state populated on the folding pathway of ubiquitin? *FEBS Lett. 567*, 333–338.
13. Vallee-Belisle, A., Turcotte, J. F., and Michnick, S. W. (2004) raf RBD and ubiquitin proteins share similar folds, folding rates and mechanisms despite having unrelated amino acid sequences. *Biochemistry 43*, 8447–8458.
14. Khorasanizadeh, S., Peters, I. D., and Roder, H. (1996) Evidence for a three-state model of protein folding from kinetic analysis of ubiquitin variants with altered core residues. *Nat. Struct. Biol. 3*, 193–205.
15. Jacob, J., Krantz, B., Dothager, R. S., Thiyagarajan, P., and Sosnick, T. R. (2004) Early collapse is not an obligate step in protein folding. *J. Mol. Biol. 338*, 369–382.
16. Gladwin, B. F., and Evans, P. A. (1996) Structure of very early protein folding intermediates: New insights through a variant of hydrogen exchange labelling. *Folding Des. 1*, 407–417.
17. Crespo, M. D., Simpson, E. R., and Searle, M. S. (2006) Population of on-pathway intermediates in the folding of ubiquitin. *J. Mol. Biol. 360*, 1053–1066.
18. Vallee-Belisle, A., and Michnick, S. W. (2007) Multiple tryptophan probes reveal that ubiquitin folds via a late misfolded intermediate. *J. Mol. Biol. 374*, 791–805.
19. Klein-Seetharaman, J., Oikawa, M., Grimshaw, S. B., Wirmer, J., Duchardt, E., Ueda, T., Imoto, T., Smith, L. J., Dobson, C. M., and Schwalbe, H. (2002) Long-range interactions within a non-native protein. *Science 295*, 1719–1722.
20. Fersht, A. R., Itzhaki, L. S., ElMasry, N. F., Matthews, J. M., and Otzen, D. E. (1994) Single versus parallel pathways of protein folding and fractional formation of structure in the transition state. *Proc. Natl. Acad. Sci. U.S.A. 91*, 10426–10429.
21. Crespo, M. D., Platt, G. W., Bofill, R., and Searle, M. S. (2004) Context-dependent effects of proline residues on the stability and folding pathway of ubiquitin. *Eur. J. Biochem. 271*, 4474–4484.
22. Platt, G. W., Simpson, S. A., Layfield, R., and Searle, M. S. (2003) Stability and folding kinetics of a ubiquitin mutant with a strong propensity for nonnative β-hairpin conformation in the unfolded state. *Biochemistry 42*, 13762–13771.
23. Kiefhaber, T., Sanchez, I. E., and Bachmann, A. (2005) Characterisation of protein folding barriers with rate equilibrium free energy relationships. In *Protein Folding Handbook. Part I* (Kiefhaber, T., and Buchner, J., Eds.) Wiley-VCH, Weinheim, Germany.
24. Gianni, S., Ivarsson, Y., Jemth, P., Brunori, M., and Travaglini-Allocatelli, C. (2007) Identification and characterization of protein folding intermediates. *Biophys. Chem. 128*, 105–113.
25. Bachmann, A., and Kiefhaber, T. (2005) Kinetic mechanisms in protein folding. In *Protein Folding Handbook. Part I* (Kiefhaber, T., and Buchner, J., Eds.) Wiley-VCH, Weinheim, Germany.
26. Fersht, A. R. (1995) Optimisation of rates of protein folding: The nucleation-condensation mechanism and its implications. *Proc. Natl. Acad. Sci. U.S.A. 92*, 10869–10873.
27. Pappenberger, G., Aygun, H., Engels, J. W., Reimer, U., Fischer, G., and Kiefhaber, T. (2001) Nonprolyl cis peptide bonds in unfolded proteins cause complex folding kinetics. *Nat. Struct. Biol. 8*, 452–458.
28. Vijaykumar, S., Bugg, C. E., and Cook, W. J. (1987) Structure of Ubiquitin Refined at 1.8 Å Resolution. *J. Mol. Biol. 194*, 531–544.
29. Munoz, V., and Serrano, L. (1997) Development of the multiple sequence approximation within the AGADIR model of α helix formation: Comparison with Zimm-Bragg and Lifson-Roig formalisms. *Biopolymers 41*, 495–509.
30. Jourdan, M., and Searle, M. S. (2000) Co-operative assembly of a native-like ubiquitin structure through peptide fragment complexation: Energetics of peptide association and folding. *Biochemistry 39*, 12355–12364.
31. Cox, J. P. L., Evans, P. A., Packman, L. C., Williams, D. H., and Woolfson, D. N. (1993) Dissecting the structure of a partially folded protein: Circular dichroism and nuclear magnetic resonance studies of peptides from ubiquitin. *J. Mol. Biol. 234*, 483–492.
32. Sharman, G. J., Griffiths-Jones, S. R., Jourdan, M., and Searle, M. S. (2001) Effects of amino acid ϕ,ψ propensities and secondary structure interactions in modulating Hα chemical shifts in peptide and protein β-sheet. *J. Am. Chem. Soc. 123*, 12318–12324.
33. Serrano, L., Neira, J. L., Sancho, J., and Fersht, A. R. (1992) Effect of Alanine Versus Glycine in α-Helices on Protein Stability. *Nature 356*, 453–455.
34. Luo, Y. Z., and Baldwin, R. L. (2001) How Ala to Gly mutations in different helices affect the stability of the apomyoglobin molten globule. *Biochemistry 40*, 5283–5289.
35. Travaglini-Allocatelli, C., Gianni, S., and Brunori, M. (2004) A common folding mechanism in the cytochrome c family. *Trends Biochem. Sci. 29*, 535–541.
36. Sanchez, I. E., and Kiefhaber, T. (2003) Origin of unusual ϕ-values in protein folding: Evidence against specific nucleation sites. *J. Mol. Biol. 334*, 1077–1085.
37. Otzen, D. E., Kristensen, O., Proctor, M., and Oliveberg, M. (1999) Structural changes in the transition state of protein folding: Alternative interpretations of curved chevron plots. *Biochemistry 38*, 6499–6511.
38. Sanchez, I. E., and Kiefhaber, T. (2003) Hammond behaviour versus ground state effects in protein folding: Evidence for narrow free energy barriers and residual structure in unfolded states. *J. Mol. Biol. 327*, 867–884.
39. Oliveberg, M., Tan, Y.-J., Silow, M., and Fersht, A. R. (1998) The changing nature of the protein folding transition state: Implications for the shape of the free energy profile for folding. *J. Mol. Biol. 277*, 933–943.
40. Roder, H., Maki, K., Latypov, R. F., Cheng, H., and Ramachandra Shastry, M. C. (2005) Early events in protein folding explored by rapid mixing methods. In *Protein Folding Handbook. Part I* (Kiefhaber, T., and Buchner, J., Eds.) Wiley-VCH, Weinheim, Germany.
41. Gladwin, S. T., and Evans, P. A. (1996) Structure of very early inytermediates: New insights through a variant of hydrogen exchange labeling. *Folding Des. 1*, 407–417.
42. Qin, Z., Ervin, J., Larios, E., Gruebele, M., and Kihara, H. (2002) Formation of a compact structured ensemble without fluorescence signature early during ubiquitin folding. *J. Phys. Chem. B 106*, 13040–13046.
43. Larios, E., Li, J. S., Schulten, K., Kihara, H., and Gruebele, M. (2004) Multiple probes reveal a native-like intermediate during low-temperature refolding of ubiquitin. *J. Mol. Biol. 340*, 115–125.
44. Gianni, S., Guydosh, N. R., Khan, F., Caldas, T. D., Mayor, U., White, G. W. N., DeMarco, M. L., Daggett, V., and Fersht, A. R. (2003) Unifying features in protein-folding mechanisms. *Proc. Natl. Acad. Sci. U.S.A. 100*, 13286–13291.
45. Gianni, S., Geierhaas, C. D., Calosci, N., Jemth, P., Vuister, G. W., Travaglini-Allocatelli, C., Vendruscolo, M., and Brunori, M. (2007) A PDZ domain recapitulates a unifying mechanism for protein folding. *Proc. Natl. Acad. Sci. U.S.A. 103*, 128–133.
46. Capaldi, A. P., Kleanthous, C., and Radford, S. E. (2002) Im7 folding mechanism: Misfolding on a path to the native state. *Nat. Struct. Biol. 9*, 209–216.
47. Li, L., Mirny, L. A., and Shakhnovich, E. I. (2000) Kinetics, thermodynamics and evolution of non-native interactions in a protein folding nucleus. *Nat. Struct. Biol. 7*, 336–342.
48. Krishna, M. M. G., and Englander, S. W. (2007) A unified mechanism for protein folding: Predetermined pathways with optional errors. *Protein Sci. 16*, 449–464.
49. Krantz, B. A., Mayne, L., Rumbley, J., Englander, S. W., and Sosnick, T. R. (2002) Fast and slow intermediate accumulation and the initial barrier mechanism in protein folding. *J. Mol. Biol. 324*, 359–371.
50. Bofill, R., and Searle, M. S. (2005) Engineering stabilising interactions into a conformationally flexible region of the folding transition state of ubiquitin. *J. Mol. Biol. 353*, 373–384.

BI800722D